

International Journal of Modern Physics D  
© World Scientific Publishing Company

## Neutrino Capture Induced Supernova Explosions

Terrance Strother

*Department of Physics and Astronomy and  
National Superconducting Cyclotron Laboratory,  
Michigan State University  
East Lansing, MI 48824, USA  
strothe6@pa.msu.edu*

Wolfgang Bauer

*Department of Physics and Astronomy and  
National Superconducting Cyclotron Laboratory,  
Michigan State University  
East Lansing, MI 48824, USA  
bauer@pa.msu.edu*

Received Day Month Year  
Revised Day Month Year  
Communicated by Managing Editor

Motivated by the success of kinetic theory in the description of observables in intermediate and high energy heavy ion collisions, we use kinetic theory to model the dynamics of core collapse supernovae. The specific way that we employ kinetic theory to solve the relevant transport equations allows us to explicitly model the propagation of neutrinos and a full ensemble of nuclei and treat neutrino-matter interactions in a very general way. With these abilities, our simulations have observed dynamics that may prove to be an entirely new neutrino capture induced supernova explosion mechanism.

*Keywords:* supernova; kinetic theory; ensemble of nuclei.

### 1. Introduction

Intermediate and high energy nuclear collisions have been very accurately modeled by simulations that made use of transport theories based on a semiclassical implementation of kinetic theory.<sup>1,2,3</sup> Given the large overlap of the requirements that must be satisfied by simulations of nuclear collisions and supernova,<sup>4,5,6</sup> such as the ability to model particle production, shock wave formation, collective deflection, as well as the interplay between regular and chaotic collective dynamics, it is tempting to implement these types of kinetic theory based approaches to model the physics and astrophysics of supernova explosions. This is the aim of our work.

As discussed in our previous work,<sup>7</sup> our code is a designed to run on large multi-processor installations and is capable of calculating all desired statistical distributions in the full three-dimensional coordinate space and propagating test particles

2 *T. Strother, W. Bauer*

in the full six-dimensional phase space. However, for debugging purposes, we also want to provide ways to test the implementation of our ideas on a single processor. The calculation discussed here is performed exactly for that purpose and is a simulation of the collapse and early stages of the explosion of a non-rotating spherically symmetric core.<sup>8</sup> While test particles are still propagated in the full six-dimensional phase space, due to statistical limitations imposed by working on a single processor,<sup>7</sup> we assume that all statistical distributions are spherically symmetric. The algorithms employed to calculate the spherically symmetric statistical distributions are discussed in detail in our previous work.<sup>7</sup>

## 2. Equations of Motion

The one-body transport equation for the baryon phase space density  $f_b(xp)$  is given by<sup>9</sup>

$$\begin{aligned} \frac{\partial f_b(xp)}{\partial t} + \frac{\Pi^i}{E_b^*(p)} \nabla_i^x f_b(xp) - \frac{\Pi^\mu}{E_b^*(p)} \nabla_i^x U_\mu(x) \nabla_p^i f_b(xp) + \frac{M_b^*}{E_b^*(p)} \nabla_i^x U_s(x) \nabla_p^i f_b(xp) \\ = I_{bb}^b(xp) + I_{b\nu}^b(xp) \end{aligned} \quad (1)$$

for the particular state  $b$  of the baryon. The left hand side of (1) describes the temporal changes in the baryon phase space density due to interactions due to the interactions of the nucleons with the mean field vector and scalar potentials  $U_\mu$  and  $U_s$ . The two source terms on the right hand side of (1) are collision integrals that that represent the effects that correlations due to the two-body baryon-baryon and baryon-neutrino collisions have the baryon phase space density respectively.

For any neutrino species, the transport equation simplifies to an equation of motion that contains only the streaming and baryon-neutrino collision terms since there are no mean field contributions and the possible effects of neutrino-neutrino collisions are neglected,

$$\frac{\partial f_\nu(xp)}{\partial t} + \frac{p \cdot \nabla^x}{E_\nu(p)} f_\nu(xp) = I_{b\nu}^\nu(xp). \quad (2)$$

It is through the baryon-neutrino collisions that the baryon and neutrino phase space densities can affect one another and the transport equations are coupled by the source terms that represent these effects.

## 3. Algorithmic Implementation

To numerically solve the coupled baryon and neutrino transport equations (1) and (2), the so-called test particle method is used.<sup>10</sup> Instead of fully discretizing the relevant six-dimensional phase space and calculating the phase space densities in each grid cell in every time step, the test particle method only follows the initially occupied phase space cells in time and represent them by imaginary test particles. These imaginary test particles are propagated in a way that models the physical

evolution of the phase space. They interact with one another via mean field one-body potentials and scatter with realistic cross sections.

The test particle method formally approximates the phase space density with a sum over delta functions

$$f(xp) = \sum_{i=0}^N \delta^3(\vec{x} - \vec{x}_i(t)) \delta^3(\vec{p} - \vec{p}_i(t)) \quad (3)$$

where  $N$  is the total number of test particles. Insertion of this approximation of the phase space density into the transport equations (1) and (2) yields simple semi-classical first-order linear differential equations of motion for the centroid coordinates of each test particle. The fact that the baryon and neutrino transport equations are solved in an identical fashion means that the treatment of neutrino dynamics is on equal footing with that of baryons. This is a significant advantage that the test particle approach has over traditional hydrodynamic models.

#### 4. Matter Test Particle Properties

Matter test particles can explicitly represent hundreds of different species of nuclei as well as free baryons. Initially the nuclear properties of the matter test particles are chosen to be consistent with the chemical composition of the progenitor.<sup>8</sup> At later times, these nuclear properties are determined by local electron capture rates and the number and type of interactions each matter test particle has with neutrino test particles. In this way, we explicitly model the propagation of an entire ensemble of nuclei and retain full knowledge of nuclear composition everywhere in the core at all times. This is superior to the standard tracking of the abundances of free protons, neutrons, alpha particles, and a “representative heavy nucleus” employed by most hydrodynamic calculations. Nuclear structure effects significantly impact electron and neutrino capture rates,<sup>11</sup> and many of these effects can be missed if one speaks of a “representative heavy nucleus” instead of an ensemble of nuclei.

Matter test particles implicitly represent electrons as well. We assume that for each proton represented by a matter test particle, free or bound in a nucleus, there is an electron nearby so that macroscopic charge neutrality is preserved. This assumption renders the matter test particles charge neutral and advantageously permits us to avoid modeling Coulomb forces between them.

Each matter test particle has its own temperature. This temperature is initially given by the temperature distribution of the chosen progenitor.<sup>8</sup> A matter test particle’s temperature can change when it comes into contact with matter test particles representing matter at different temperatures, or when the electrons it implicitly represents are part of an electron gas that is heated or cooled by weak reactions involving electrons.

For the purposes of calculating gravitational forces and density distributions, all matter test particles are assigned the same average mass. This average mass is taken to be the mass of the core divided by the number of matter test particles used to model it.

4 *T. Strother, W. Bauer*

After the insertion of the delta function approximation of the baryon phase space density into equation (1), it is found that the centroid of each matter test particle is subject to three mean field forces: a gravitational force, a nucleonic force, and a force exerted by the surrounding electron gas on the electrons it implicitly represents. Matter test particles can also scatter with one another. The equations of motion for the centroid coordinates of the matter test particles are given by the following first order differential equations

$$\frac{d}{dt}\vec{p}_j = \vec{F}_G(\vec{r}_j) + \vec{F}_{nuc}(\vec{r}_j) + \vec{F}_{e^-}(\vec{r}_j) + \vec{C}(\vec{p}_j) \quad (4)$$

$$\frac{d}{dt}\vec{r}_j = \frac{\vec{p}_j}{\sqrt{m^2 + p_j^2}} \quad (5)$$

$$j = 1, \dots, N$$

where  $\vec{F}_{G,j}$  is the gravitational force acting on the  $j^{th}$  matter test particle,  $\vec{C}(\vec{p}_j)$  symbolizes the effects that two-body collisions with other matter test particles have on the  $j^{th}$  matter test particle's momentum, and  $N$  is the number of matter test particles used to model the core and is constant.

## 5. Matter Test Particle Interactions

Single processor simulations that assume that statistical distributions are spherically symmetric model gravitation with a modified Newtonian monopole algorithm discussed in our previous works.<sup>12</sup> The mean field nucleonic and electron gas forces a matter test particle is subject to are taken to be the average force that would be exerted on a nucleon or electron sitting at its centroid by the surrounding gas of nucleons or electrons multiplied by the number of nucleon or electrons it represents. For nucleons, this average force is taken to be  $-\vec{\nabla}U_{nuc}$ , where  $U_{nuc}$  is a mean field nucleon potential. For now we approximate the nucleon mean field potential with simple density dependent functionals. For electrons, this average force is taken to be  $-1/n_e \cdot \vec{\nabla}P_e$ , where  $n_e$  and  $P_e$  are the local electron number density and finite temperature pressure exerted by a relativistic gas of electrons respectively. The former quantity is readily calculable and the latter is interpolated from a table.

In addition to the forces that matter test particles directly and indirectly exert on one another, they can scatter off other nearby matter test particles. The way we model test particle scattering is explained at length in our previous work.<sup>13</sup> Here it suffices to say that test particle scatterings are modeled relativistically and semi-classically in a way similar to those used in the simulation of heavy ion collisions.<sup>14</sup>

## 6. Neutrino Test Particle Properties

Unlike matter test particles, the number of neutrino test particles is not constant. Neutrino test particles can be created and destroyed. The latter process can be

induced by a weak interaction or by a neutrino test particle escaping the core. The number of neutrino test particles therefore varies greatly at different times during the simulation. The only neutrino production mechanism currently included in our model is electron capture by nuclei and free protons. Since it is easy to demonstrate that neutrino flavor oscillations are strongly suppressed in the core,<sup>15</sup> only the presence of electron neutrinos is currently simulated. It is clear how to include other neutrino production mechanisms into our model as well as how to model the presence of all flavors of neutrinos and anti-neutrinos, but we have elected to proceed incrementally when constructing the weak reaction network for this completely new model.

Neutrino test particles are assumed to be massless, move at the speed of light, and subject to no mean-field-type forces. The only way they can interact with other test particles is through scattering with or being captured by matter test particles. Thus the propagation of neutrino test particles between weak reaction sites is quite simple. Merely multiplying the intermediate unit momentum vector of a neutrino test particle by the speed of light and propagation time determines its new location. No complicated numerical method of approximating the solutions to differential equations is required. This light speed propagation does put limits in on the time step size. To realistically model the propagation of neutrino test particles within the constraints of our coordinate space cells, the time step size should be no larger than  $10^{-5}$  s.

## 7. Neutrino Test Particle Creation

Currently we use the widely available Fuller-Fowler-Newman (FFN) table<sup>16</sup> as the source for our electron capture rates. We extrapolate the rates from the FFN table to the nuclei not included in their table that we include in our simulation, and then reduce all entries by an order of magnitude. Our motivation for doing this is as follows. More recent calculations of weak reaction rates using new shell models of the distribution of Gamow-Teller strength have resulted in an improved and often reduced estimate of its strength compared to those the FFN calculations yielded using extrapolations of the known experimental rates and a simple single-state representation of this resonance.<sup>17</sup> The difference is often an order of magnitude or more, so this table serves as a reasonable estimate of the rates.

## 8. Neutrino Test Particle Interactions

Beam attenuation arguments are ideally suited for calculating neutrino-matter interaction probabilities for neutrinos represented by a neutrino test particle. Thus we take the probability that the neutrinos represented by a neutrino test particle that moves from location  $\vec{x}_1$  to  $\vec{x}_2$  to be given by

$$P_{int} = 1 - \exp \left[ - \int_{\vec{x}_1}^{\vec{x}_2} \sum_i \bar{\sigma}_i(\vec{x}') n_i(\vec{x}') d\vec{x}' \right] \quad (6)$$

6 *T. Strother, W. Bauer*

where the sum over  $i$  runs over all of the interaction channels available to the neutrino test particles encounters between its initial and final locations,  $n_i$  is the local number density of the  $i^{\text{th}}$  species of particle, electrons, free baryons, or nuclei, and  $\bar{\sigma}_i$  is the average effective interaction cross section corresponding to the  $i^{\text{th}}$  interaction channel.<sup>18</sup> The  $n_i$ 's are readily calculable and the  $\bar{\sigma}_i$ 's are interpolated from tables.

Once the interaction probability (6) is calculated, a simple Monte-Carlo algorithm determines if the neutrino test particle interacts with matter. Interaction channels are selected by constructing relative probabilities out of weighted average effective cross sections and using another simple Monte-Carlo algorithm to choose a channel. The significant appeal that this very general way of modeling neutrino-matter interactions is that it is applicable everywhere in the core. This is a major advantage this kinematic model has over its hydrodynamic counterparts. Typical hydrodynamic treatments of neutrinos are well justified only in the extremely short and long mean free path limits and are quite problematic at intermediate values.<sup>19,20</sup>

## 9. New Dynamics

All of our most recent simulations have observed new dynamics that may prove to be an entirely new neutrino capture induced supernova explosion mechanism. The early stages of the collapse calculated by our code unfold identically to the accepted picture of supernova collapse. Electron capture rates initially slowly increased as the collapse progressed and at later times rapidly increased and eventually led to rapid deleptonization of the inner core. Not long after the inner region of the core begins to rapidly deleptonize, an unexpected phenomenon is observed in each calculation. In all of our simulations it is always found that neutrino captures at intermediate radii inside the inner region of the core deposits a large amount of electrons in a narrow spherical shell centered about a radius of approximately 45-55 km. This radially localized accumulation of electrons alters the electron number density gradient in such a way that substantially increases the outward pressure exerted by the electron gas in the region just outside the radius at which the most electrons are produced. The resultant electron gas pressure profile generates an outward explosion of matter at radii of approximately 55 km. Matter inside this region always collapses inward and formed a proto-remnant.

This accumulation of electrons produced by neutrino capture is most easily seen in a plot of the electron fraction distribution. In Fig. 1 we show a plot of the electron fractions in the spherical shells used to calculate statistical distributions. The distribution is generated after the outward explosion of matter is well underway, and the impact that localized production of electrons has on the electron fraction distribution is apparent. It is clear the accumulation of electrons produced by neutrino capture manifests itself as a well defined spike in the electron fraction distribution. Results similar to this were produced by each calculation.

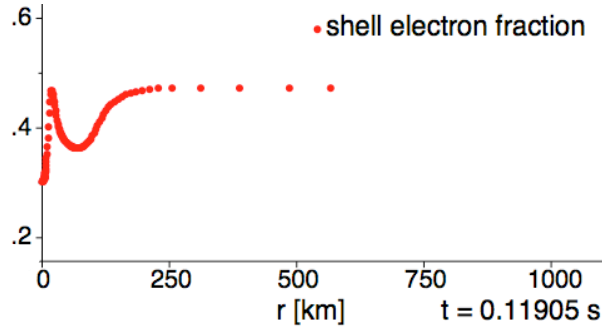


Fig. 1. Plot of the electron fractions in the spherical shells after the outward explosion of matter is well underway.

## 10. Analysis of New Dynamics

This neutrino capture induced explosion mechanism substantially differs from the accepted bounce mechanism in many ways. The density in the region where the outward explosion of matter forms was always found to be on the order of  $10^{-3}$  nuclear matter density while the central densities at that time were consistently found to be on the order of 0.1 nuclear matter density. This is a significant deviation from the accepted picture of bounce in which the initial outward explosion of matter is generated by the pressure exerted by matter at supernuclear densities accumulated in a small volume near the origin. Thus the role of the nuclear equation of state is fundamentally different in this scenario. Rather than directly dictating how the outward explosion of matter is formed by determining the maximum density the central region can assume, it indirectly influences the neutrino capture induced explosion by governing the rate at which electron capture occurs that power the explosion.

The confluence of events that lead to the radial localization of the neutrino captures are well understood. An in depth discussion of them is beyond the scope of this article. Here it suffices to say that the origin of this phenomenon are rooted in weak reactions, nuclear structure effects and relativistic quantum electron gas statistical mechanics. Our ability to observe this phenomenon is critically dependent on our ability to propagate a full ensemble of nuclei and most importantly our ability to realistically model neutrino-matter interactions at intermediate densities.

## 11. Summary

We are encouraged by these results generated by our kinetic theory based model. The neutrino capture driven mechanism that it is uniquely poised to observe is robust enough to launch explosions in all simulations conducted so far using three different nucleon potentials, four different versions of the electron capture rate table described in section 7, and three different numbers of spherical shells used to

8 *T. Strother, W. Bauer*

calculate statistical distributions. However we realize that in addition to converting the code to 64-bit and parallelizing it, activating the three-dimensional subroutines, and conducting more numerical convergence tests, there is still more physics that needs to be added to our model. In particular, fusion and photodisintegration must be built in as do several additional weak reactions. It is clear how to accomplish all of this with the test particle approach.

We are confident that this new explosion mechanism will survive the implementation the aforementioned physics. The additional degrees of freedom introduced when three-dimensional distributions are calculated may destabilize the region in which electron are deposited by neutrino capture as it may be unstable to convection. An entropy analysis can confirm if this is a possibility. However even if convection does destabilize this region, the fact that convection begins at only  $\sim 1100$  ms after the collapse begins at a radius on the order of 50 km would be a significant discovery in and of itself. The future of this model looks extremely bright and we look forward to continuing to advance it.

## References

1. G.F. Bertsch et al., *Phys. Rev. C* **29**, (1984) 673.
2. H. Kruse et al., *Phys. Rev. Lett.* **54**, (1985) 289.
3. W. Bauer, G.F. Bertsch, W. Gassing, and U. Mosel, *Phys. Rev. C* **34**, (1986) 2127.
4. J.R. Wilson, *Numerical Astrophysics*, (Jones and Bartlett, Boston, 1985).
5. M. Herant, W. Benz, W. Hix, C. Fryer, and S. Colgate, *Astrophys. J.* **435**, (1994) 339.
6. C.L. Fryer and A. Heger, *Astrophys. J.* **541**, (2000) 1033.
7. T. Strother and W. Bauer, *Prog. Part. Nucl. Phys.*, **62**, (2009) 468.
8. S.E. Woosley and T.E. Weaver, *Ann. Rev. Astron. Astrophys.* **24** (1986) 205.
9. W. Bauer, *Acta Phys. Hung. A* **21**, (2004) 371.
10. C.-Y. Wong, *Phys. Rev. C* **25** 1460 (1982).
11. G. Matr inez, M. Liebend rfer, and D. Frekers, *Nucl. Phys. A*, (2004).
12. W. Bauer and T. Strother, *Int. J. Mod. Phys. E* **14**, (2005) 129.
13. T. Strother and W. Bauer, Nuclear physics and supernova explosions: Unified dynamics., to appear in *Int. J. Mod. Phys. D*
14. G. Kortemeyer, F. Daffin, and W. Bauer, *Phys. Lett.* **B374**, (1996) 25.
15. L. Wolfenstein, *Phys. Rev. D*, **17**, (1978) 2369.
16. G. Fuller, W. Fowler, and M. Newman, *Astrophys. J.*, **293** 1, (1985).
17. A. Heger and S. E. Woosley, *Astrophys. J.*, **560**, 307, (2001).
18. A. Burrows and T. Thompson, *Astrophys. J.* (2002).
19. M. Herant, W. Benz, and S. Colgate, *Astrophys. J.*, **395**, 642, (1992).
20. M. Herant, W. Benz, W. Hix, C. Fryer and S. Colgate, *Astrophys. J.*, **435**, (1994).